Accepted manuscript at https://doi.org/10.1016/j.medengphy.2019.12.006

Application of an OCT-based 3D reconstruction framework to the hemodynamic assessment of an ulcerated coronary artery plaque

Susanna Migliori[1,2], Claudio Chiastra[2,3], Marco Bologna[2,4], Eros Montin[4,5], Gabriele Dubini[2], Lorenzo Genuardi[6], Cristina Aurigemma[6], Luca Mainardi[4], Francesco Burzotta[6], Francesco Migliavacca[2]

1. Research and Development Department, Caristo Diagnostics, Oxford, UK
2. Laboratory of Biological Structure Mechanics (LaBS), Department of Chemistry, Materials and Chemical Engineering "Giulio Natta", Politecnico di Milano, Milan, Italy
3. PoliTo^{BIO}Med Lab, Department of Mechanical and Aerospace Engineering, Politecnico di Torino, Turin, Italy
4. Department of Electronics, Information and Bioengineering, Politecnico di Milano, Milan, Italy
5. Center for Advanced Imaging Innovation and Research (CAI2R), and the Bernard and Irene Schwartz Center for Biomedical Imaging, Department of Radiology, New York University School of Medicine, New York, NY, USA;
6. Institute of Cardiology, Fondazione Policlinico Universitario A. Gemelli IRCCS, Università Cattolica del Sacro Cuore, Rome, Italy

Address for correspondence:

Prof. Francesco Migliavacca

Laboratory of Biological Structure Mechanics (LaBS)

Department of Chemistry, Materials and Chemical Engineering "Giulio Natta"

Politecnico di Milano

Piazza Leonardo da Vinci 32

20133 Milan, Italy

E-mail: francesco.migliavacca@polimi.it

Post-print

Accepted manuscript at https://doi.org/10.1016/j.medengphy.2019.12.006

Abstract

The rupture of a vulnerable plaque, ulceration, is the most common cause of myocardial infarction. It can be recognized by angiographic features, such as prolonged intraluminal filling and delayed clearance of the contrast liquid. The diagnosis of such an event is an open challenge due to the limited angiographic resolution and acquisition frequency. The treatment of ulcerated plaques is an open discussion, due to the high heterogeneity and the lack of evidences that support particular strategies. Therefore, the therapeutic decision should follow a detailed investigation with angiography and intravascular imaging, such as optical coherence tomography (OCT), to locate the lesion, besides its geometric features and the lumen occlusion severity.

The aim of this study is the application of a framework for the in-silico analysis of the disrupted hemodynamics due to an ulcerated lesion. The study employed a validated OCT-based reconstruction methodology and computational fluid dynamics (CFD) simulations for the computation of local hemodynamic quantities, such as wall shear stress.

The achieved findings, such as disrupted pre-operative flow conditions, proved the applicability of the developed framework for CFD analyses on complicated patient-specific anatomies that feature ulcerated plaques. The prediction of lesion expansion and the clinical decision making can benefit from a reliable computation of wall shear stress distributions that result from the peculiar anatomy of the lesion. Therefore, the application of intravascular OCT imaging, high fidelity 3D reconstructions and CFD simulations might guide the treatment of such pathology.

Post-print

Keywords

Optical coherence tomography, image segmentation, coronary artery, ulcerated plaque, pre-operative assessment, patient-specific modelling, computational fluid dynamics, wall shear stress

Highlights

- Semi-automatic segmentation of pre- and post-operative OCT images.
- 3D modelling of an ulcerated coronary artery lesion from OCT and angiography.
- Pre- and post-operative patient-specific CFD model of an ulcerated coronary artery.

Abbreviations

CAD: Computer-aided design

CFD: Computational fluid dynamics

DICOM: Digital Imaging and COmmunications in Medicine

MB: Main branch

OCT: Optical coherence tomography

PCI: Percutaneous coronary intervention

3D-QCA: 3D quantitative coronary angiography

RCA: right coronary artery

SB: Side branch

TAWSS: Time-averaged wall shear stress

WSS: Wall shear stress

Post-print

1. Introduction

Coronary artery disease is the most frequent cause of death and disability in the Western Countries [1]. Typically, this disease is the consequence of the formation of an atherosclerotic plaque within the coronary artery wall. Post-mortem analyses reported in the literature demonstrate that the majority of myocardial infarctions are induced by the rupture of coronary plaques in association with thrombotic arterial occlusions [2]. Therefore, an accurate identification of vulnerable plaques is crucial in order to prevent such events. The employment of intra-vascular imaging modalities enables a reliable lesion classification, through a high resolution picture of the plaque composition [3]. Moreover, post-mortem studies have revealed that high risk plaques with thin-cap fibroatheromas can be distinguished from stable lesions as they are characterized by a larger necrotic core [4]. Such type of lesion has features that can be exclusively captured with intra-vascular imaging modalities. The fracture of the thin-cap results in a plaque ulceration, which can be recognized also by angiographic features, due to a prolonged intraluminal filling and delayed clearance of the contrast liquid. The guidelines for treatment of plaque ulceration relies on catheter-based perfusion of the diseased artery and percutaneous coronary intervention (PCI). The identification of the plaque composition is not regularly monitored due to the low image resolution of established imaging modalities, such as coronary angiography [5]. On the contrary, the near-histological resolution of intravascular optical coherence tomography (OCT) provides detailed pictures of the vessel wall, allowing an accurate characterization of the plaque and the possibility to perform in-vivo detailed reports of this high-risk pathology [2].

The treatment of ulcerated plaques is an open discussion, due to the high geometry heterogeneity, depth and extension, and the lack of indications that support particular strategies [6]. Stent deployment is suggested for plaques with relevant degree of lumen narrowing (70-90%) and in association with unstable conditions. Although intravascular images after PCI commonly show good lesion coverage and stent apposition, in some cases the intramural hematoma is persistent at the scaffolded region and at the distal extremity of the stent [7].

The knowledge of lesion geometry might lead to case-specific decision making approach. In particular, the peculiar flow conditions across an ulcerated plaque can be investigated via computational fluid dynamics (CFD) simulations. In this study, we applied an in-silico framework for the modelling of patient-specific hemodynamics to analyze the effect of an ulcerated plaque on the blood flow. Both the pre- and post-operative scenario was investigated by reconstructing a patient-specific 3D model from OCT and angiographic images.

2. Materials and methods

A 70-year-old man was found with ulcerated plaque and 70% stenosis (minimum lumen area of 2.5 mm^2) at the distal right coronary artery (RCA). The occlusive lesion was treated with direct stenting at the Institute of Cardiology, Catholic University of the Sacred Heart (Rome, Italy). Specifically, a 3.5x24 mm Nobori Stent (Terumo Corp., Tokyo, Japan) was deployed in the diseased coronary segment and post-dilated with a 4x15 mm angioplasty balloon. The study complies with the Declaration of Helsinki on human research and was approved by Catholic University of the Sacred Heart Ethics Committee. All patients gave informed consent.

The OCT images acquired both before and after PCI were processed as described in the work of Migliori et al. [8] to retrieve high fidelity 3D models of (i) the diseased (i.e. pre-operative) and (ii) treated (i.e. post-operative) coronary bifurcated segment. The reconstructed 3D models were used to perform CFD analyses. Local hemodynamic quantities, such as the wall shear stress (WSS) along the arterial lumen, were computed.

2.1 Three-dimensional geometry reconstruction

The blood vessel was imaged with a C7-XR Fourier-Domain OCT system (St. Jude Medical, St. Paul, MN, USA) comprising a C7 Dragonfly catheter (St. Jude Medical). The maximum length of the analyzed segment was 54 mm with a frame rate of 180 frames per second. The OCT system ensured axial resolution of 12-18 μm and lateral resolutions of 20-90 μm; the pull-back resolution was 100 μm. A total of 540 frames per scan were recorded in DICOM format (1024x1024 pixels). Figure 1 shows an OCT frame of the ulceration, which caused the generation of a false lumen (blue seven-pointed star) besides the true lumen (green five-pointed star).

The employed 3D reconstruction methodology was performed in a MATLAB environment (Mathworks, Natick, MA, USA) and comprised two phases: (i) image elaboration for the detection of the lumen contour and stent struts, (ii) alignment and orientation of the detected components with the vessel centerline, obtained from angiography. The implemented methodology is described in detail elsewhere [8–10]. A brief description of the main reconstruction steps is presented below.

Each OCT frame was processed in polar coordinates. The images were pre-processed to reduce the noise in the vessel lumen and to remove the OCT catheter. An intensity thresholding and morphological

Post-print

operations on the images were applied to retrieve the arterial wall. The edges were detected by means of a Sobel filter, the innermost lumen border was defined as the set of the first edge pixels for each image column (i.e. for each A-scan). These pixels were interpolated and converted to Cartesian coordinates and were stored as points on bidimensional (2D) planes. The metallic stent struts reflected the near-infrared light of the OCT A-scan and they appeared as bright elements followed by a trailing shadow (i.e. low intensity region). This feature was identified by the slope of a line connecting each peak in the image intensity profile with the thirtieth consecutive low intensity pixel, as previously proposed [11]. Pixels that resulted with higher slope values were considered part of a strut. False positives were discarded by means of a mask that reflected the probability of a pixel to be part of a strut. The mask values at the lumen border were 1 and decreased to 0 moving towards the lumen center, and were 0 below the contour. A further correction comprised the application of a confidence region that introduced a continuity in the stent geometry, by means of the information from the surrounding 5 images in order to build a smooth curve. In particular, pixels candidates that laid outside this tolerance region were discarded. Finally, each image was converted to Cartesian coordinates and stent struts centroids were recorded as points in the 2D planes.

The detected components were aligned with the 3D vessel centerline that was obtained from two angiographic projections. In particular, the angiographic images were processed using the commercial software CAAS (PIE Medical Imaging BV, Maastrich, The Netherlands). The angiographic frames selected for the centerline extraction were taken at the end of the diastolic phase of the cardiac cycle, as the coronaries are filled by the contrast liquid and clearly visible. This last was used to reconstruct the 3D main branch (MB) with the implanted stent from the processed OCT images. The 3D reconstruction of the coronary segment with bifurcations was performed with Rhinoceros v.5 (Robert McNeel & Associates, Seattle, WA, USA). The side branches (SBs) were reconstructed from information achieved with a 3D quantitative coronary angiography (3D-QCA) that was carried out with CAAS (PIE Medical Imaging). Briefly, the SB circular-shaped cross-section was created by scaling the MB cross-section area to preserve the ratio between MB and SB cross-section areas of the 3D-QCA geometry. The length of each SB was 2.5 times the SB cross-section diameter.

The 3D geometry of the stent was achieved from the skeleton of the stent in its straight undeformed configuration that was morphed over the stent OCT point-cloud using Hypermesh (Altair Engineering, Inc., Troy, MI, USA). Square-shaped cross-section curves with side length of 125 μm were positioned along the morphed stent skeleton with the graphical algorithm editor Grasshoper®

Post-print

(www.grasshopper3d.com) to obtain the patient-specific stent geometry.

Figure 2 shows the final 3D reconstruction of the diseased RCA and the ulcerated plaque, which is characterized by a false lumen in the arterial wall. Figure 3 depicts the post-operative 3D geometry of the treated coronary artery segment with bifurcations.

2.2 Computational fluid dynamic simulations

The pre-operative 3D geometry was discretized using 1,849,596 tetrahedral elements with ICEM CFD v.16 (ANSYS Inc., Canonsburg, PA, USA). The region characterized by ulcerated plaque was discretized with a high density mesh (Fig. 2C). This allowed a good representation of the local flow conditions while preserving limited computational costs. The post-operative 3D geometry was discretized in 6,825,984 tetrahedral elements. The mesh size allowed a good characterization of the blood flow at both stented and side branch regions and it was defined according to a mesh independence study that was previously performed as in [12].

Transient CFD analyses were performed using Fluent v.16 (ANSYS Inc.). A typical human RCA flow waveform [13] was applied as a paraboloid-shaped velocity profile to the inlet surface [12] of both models. The average value in time was defined so that the flow-rate was 64.32 ml min^{-1} for the diseased vessel and 90.96 ml min^{-1} after stent deployment. These values were computed by means of the relationship introduced by Sakamoto and co-authors [14], that accounts for the number of angiographic cine frames that captured the flow of the radio-opaque contrast liquid in the coronary artery segment. At the outlet surfaces a zero-pressure condition was set. No slip-condition was applied to the arterial and stent walls, which were defined as rigid. A coupled solver was employed with a second-order upwind scheme for spatial discretization and a second-order implicit scheme was used for time integration. A time step of 0.009 s was chosen for performing the simulations, resulting in 100 time steps for the simulated cardiac cycle [12]. The blood was described as an incompressible non-Newtonian fluid, implementing a Bird-Carreau constitutive law with μ_∞=0.0035 kg m^{-1} s^{-1}, μ_0 = 0.25 kg m^{-1} s^{-1}, k=25 s, n=0.25 and density of 1060 kg m^{-3} [15].

For each case, the velocity field within the domain was evaluated at the peak of flow rate in order to detect the presence of abnormal fluid dynamic patterns, such as recirculation zones and vortexes. Then, the patterns of time-averaged WSS (TAWSS) were assessed. The percentages of the lumen surface area that were exposed to intervals of TAWSS between 0 Pa and 10 Pa were computed. Such analysis provided quantitative information about the global WSS spectrum at the endothelium before PCI. The analysis of

Post-print

the WSS after stent deployment was focused on regions exposed to very low TAWSS (i.e. TAWSS ≤ 0.4 Pa), considered as a potential trigger for in-stent-restenosis [16]. The TAWSS was used as primary metric of interest because it was recently shown that the hemodynamics of coronary arteries is characterized by low WSS multi-directionality as a consequence of helical flow structures with high helicity intensity that stabilize the blood flow [17].

3. Results

Figure 4 depicts the 3D streamlines of the blood velocity that was caused by a peak of the flow rate at the inlet surface in the pre-operative model (Fig. 4A). The increase of the lumen cross-section area distal to the lesion resulted in large recirculation (Fig. 4B). Flow vortexes were found in the false lumen (Fig. 4D) and at the interface with the true lumen (Fig. 4C). The planar section of the ulceration showed an abnormal vessel shape, with discontinuous intra-luminal space.

In Fig. 5 the contour map of TAWSS is shown. The reduced lumen cross-section area at the diseased region caused values of TAWSS above 10 Pa (0.49% of the total lumen area). On the other hand, the lumen surface at the vessel enlargement experienced TAWSS below 0.4 Pa (16.34% of the total lumen area). The lumen regions exposed to low and moderate TAWSS values were reported in blue and green, respectively; whereas lumen areas exposed to high TAWSS were displayed in in gray and red. The superficial distribution of TAWSS at the ulceration reflected the variable flow stream in this region.

Results from the simulated hemodynamics after PCI are reported in Figs. 6 and 7. In Fig. 6, the smooth lumen surface and the well apposed stent struts gave a flow stream without recirculation. The distribution of TAWSS in Fig. 7 presented mainly values higher than 1 Pa. Only 1.8% of the area of the scaffolded MB experienced TAWSS lower than 0.4 Pa. The resultant local fluid dynamic quantities revealed a well recovered flow. Such finding was confirmed by post intervention intravascular OCT images that revealed a recovery of the pre-atherosclerotic blood flow in the entire length of the lesion. Moreover, the images showed that the stent was implanted in the true lumen and no evidence of any residual false lumen was found.

4. Discussion

The described framework was successfully applied to study the effect of an ulcerated plaque on the local flow patterns, as well as the recovered downstream flow after PCI was examined with CFD simulations. Results revealed a high degree of flow recirculation both at the ulceration and at the interface with the

Post-print

normal lumen. The lack of clinical practice guidelines makes the treatment of non-occlusive plaques an open question. The application of advanced intra-coronary images, high fidelity reconstructions and CFD simulations might guide the management of such pathology.

The achieved findings proved the benefit of the developed framework for CFD analyses on complicated patient-specific anatomies, such as ulcerated plaques. A picture of the pre- and post-operative flow conditions and the resultant WSS distributions were achieved and the positive impact of stent implantation was proven as it enabled to restore the physiological flow conditions. Potentially, the proposed approach can be applied for the prediction of the expansion of ulceration through the intra-mural space, as WSS might provide indexes of local wall failure.

Currently, it is not available a unique guidance for the treatment of plaque ulcerations, due to the lack of evidences that define a preferable procedure. This is due to the high heterogeneity of plaque ulcerations, both in terms of pathological and geometrical features, alongside the limited number of registered cases [18]. The knowledge of lesion features, such as the peculiar geometry, leads to a patient-specific decision making approach. In this scenario, the proposed framework can represent a relevant supporting tool as it combines the advantages of a near-histological imaging technique (i.e. OCT) and CFD to emulate patient's blood flow within the considered coronary artery segment.

From a clinical point of view, this study demonstrates that in case of ulcerated plaque the stent deployment enables to recovery the pre-atherosclerotic local flow conditions with a significant extent of vessel area exposed to TAWSS values above 1 Pa (Fig. 7). This finding underlines the importance of fluid dynamics analysis for the management of such clinical conditions. For instance, similar analyses were applied in the literature to predict the failure of aneurysms. Steinman et al. [19] simulated the blood flow in an intracranial aneurysm reconstructed from computed rotational angiography. The prediction of WSS associated to the anatomy of the disease could assist the assessment of wall growth and rupture, as well as the clinical decision making.

Nevertheless, the accuracy of the study was affected by some limitations that are present in the vessel reconstructions and in the fluid dynamic models. The main limitation of the reconstruction methodology was due to the distortions of the OCT images. Indeed, the OCT pull-back was not gated by electrocardiography. Therefore, the vessel deformations induced by heart contractions were not minimized. This aspect remains an open issue due to the lack of valid algorithms for the correction of these heart motion artifacts [20]. Concerning the simulation of patient's hemodynamics, a reference pressure was prescribed at the outlets as the patient-specific flow distribution was not available.

Post-print

Moreover, the assumption of rigid vascular wall by neglecting the compliance and the cardiac-induced motion of the vessel might have affected the accuracy of the results. However, several computational studies showed that the overall TAWSS spatial distribution is preserved when analyzing non-stented coronary artery models with rigid walls [21–24]. Few studies have proposed fluid-structure interaction (FSI) models to simulate the flow in stented coronary arteries until now [25,26]. Chiastra et al. [25] proposed a FSI model comprising an idealized straight coronary segment with a stent and showed that the TAWSS distribution is minimally affected by the rigid wall assumption. Bukač et al. [26] performed FSI simulations in idealized curved coronary segment models comprising several designs of the implanted stent. The models included both the compliance of the vessel wall and the deformations due to the beating heart. The effects of each stent design to the wall and flow was investigated, and a comparison between FSI and rigid CFD simulations was not conducted. Thus, the relationship between the wall compliance and the estimated hemodynamic metrics was not investigated. In general, the FSI models are promising tools for a more accurate investigation of the hemodynamics within the coronary arteries, however their computational costs are considerably higher than CFD models and the available technology limits to apply FSI for numerical simulations. Moreover, the literature has not reported evidences that define a preferable computational model to simulate the hemodynamics in blood vessels until now.

5. Conclusions

This study presented the use of a semi-automatic OCT-based reconstruction methodology for the evaluation of blood flow disruption due to an ulcerated plaque. A high fidelity reconstruction of the lesion was achieved from the elaboration of OCT and angiography images. Patient-specific flow conditions were estimated from medical images and were used to perform in-silico analysis of the pre-operative hemodynamics. The final stent and vessel configuration after PCI were reconstructed from post-operative OCT images. The stent design and the interaction with the lumen surface were resembled. The hemodynamics was analyzed by means of a CFD simulation and the results showed a good recovery of the downstream flow after the stenting procedure.

The identification of plaque with ulceration is challenging and the definition of treatment guidelines is an open debate due to the large anatomic variability. In this context, this work is a valuable application of a framework for the in-silico analysis of the disrupted hemodynamics due to an ulcerated lesion, as well as the evaluation of post-PCI flow conditions.

Post-print

The described work can be considered as an application of a patient-specific CFD model for the blood flow characterization before and after stent implantation of a coronary vessel with ulcerated plaque. The results achieved from the reported study are promising and encourage to employ the described framework to other coronary artery cases characterized by complex lesion anatomy, as a future work.

Acknowledgements

Susanna Migliori, Francesco Migliavacca, and Gabriele Dubini were supported by the European Commission through the H2020 Marie Skłodowska-Curie European Training Network H2020-MSCA-ITN-2014 VPH-CaSE, www.vph-case.eu, GA No. 642612.

Conflict of interest

The authors have no professional or financial conflicts of interest to disclose.

Ethical approval

The analysis was approved by the Ethics Committee of the Catholic University of the Sacred Heart and conformed to the Helsinki Declaration on human research of 1975, as revised in 2000. Informed consent was obtained from the patient for being included in the study. No animal studies were carried out by the authors for this article.

References

[1] Benjamin EJ, Virani SS, Callaway CW, Chamberlain AM, Chang AR, Cheng S, et al. Heart Disease and Stroke Statistics—2018 Update: A Report From the American Heart Association. Circulation 2018;137. doi:10.1161/CIR.0000000000000558.

[2] Genuardi L, Burzotta F, Vergallo R, Crea F. Plaque erosion causing ST-segment elevation myocardial infarction. Coron Artery Dis 2017;28:355–7. doi:10.1097/MCA.0000000000000463.

[3] Jia H, Abtahian F, Aguirre AD, Lee S, Chia S, Lowe H, et al. In Vivo Diagnosis of Plaque Erosion and Calcified Nodule in Patients With Acute Coronary Syndrome by Intravascular Optical Coherence Tomography. J Am Coll Cardiol 2013;62:1748–58. doi:10.1016/j.jacc.2013.05.071.

[4] Obaid DR, Calvert PA, Brown A, Gopalan D, West NEJ, Rudd JHF, et al. Coronary CT

Post-print

angiography features of ruptured and high-risk atherosclerotic plaques: Correlation with intra-vascular ultrasound. J Cardiovasc Comput Tomogr 2017;11:455–61.

[5] Prati F, Uemura S, Souteyrand G, Virmani R, Motreff P, Di Vito L, et al. OCT-Based Diagnosis and Management of STEMI Associated With Intact Fibrous Cap. JACC Cardiovasc Imaging 2013;6:283–7. doi:10.1016/j.jcmg.2012.12.007.

[6] Mishra TK, Mishra C, Das B. An approach to the classification, diagnosis and management of vulnerable plaque. J Indian Coll Cardiol 2013;3:57–66. doi:10.1016/j.jicc.2013.03.007.

[7] Lassen JF, Holm NR, Stankovic G, Lefèvre T, Chieffo A, Hildick-Smith D, et al. Percutaneous coronary intervention for coronary bifurcation disease: consensus from the first 10 years of the European Bifurcation Club meetings. EuroIntervention 2014;10:545–60. doi:10.4244/EIJV10I5A97.

[8] Migliori S, Chiastra C, Bologna M, Montin E, Dubini G, Aurigemma C, et al. A framework for computational fluid dynamic analyses of patient-specific stented coronary arteries from optical coherence tomography images. Med Eng Phys 2017;47:105–16. doi:10.1016/j.medengphy.2017.06.027.

[9] Chiastra C, Montin E, Bologna M, Migliori S, Aurigemma C, Burzotta F, et al. Reconstruction of stented coronary arteries from optical coherence tomography images: Feasibility, validation, and repeatability of a segmentation method 2017;12:e0177495. doi:10.1371/journal.pone.0177495.

[10] Migliori S, Rampat R, Bologna M, Montin E, Burzotta F, Hildick-Smith D, et al. A Patient-Specific Study Investigating the Relation between Coronary Hemodynamics and Neo-Intimal Thickening after Bifurcation Stenting with a Polymeric Bioresorbable Scaffold. Appl Sci 2018. doi:10.3390/app8091510.

[11] Wang A, Eggermont J, Dekker N, Garcia-Garcia HM, Pawar R, Reiber JHC, et al. Automatic stent strut detection in intravascular optical coherence tomographic pullback runs. Int J Cardiovasc Imaging 2013;29:29–38. doi:10.1007/s10554-012-0064-y.

[12] Chiastra C, Morlacchi S, Gallo D, Morbiducci U, Cárdenes R, Larrabide I, et al. Computational fluid dynamic simulations of image-based stented coronary bifurcation models. J R Soc Interface 2013;10. doi:10.1098/rsif.2013.0193.

[13] Davies JE, Whinnett ZI, Francis DP, Manisty CH, Aguado-Sierra J, Willson K, et al. Evidence of a Dominant Backward-Propagating “Suction” Wave Responsible for Diastolic Coronary

Post-print

Filling in Humans, Attenuated in Left Ventricular Hypertrophy. Circulation 2006;113.

[14] Sakamoto S, Takahashi S, Coskun AU, Papafaklis MI, Takahashi A, Saito S, et al. Relation of distribution of coronary blood flow volume to coronary artery dominance. Am J Cardiol 2013;111:1420–4. doi:10.1016/j.amjcard.2013.01.290.

[15] Caputo M, Chiastra C, Cianciolo C, Cutrì E, Dubini G, Gunn J, et al. Simulation of oxygen transfer in stented arteries and correlation with in-stent restenosis. Int j Numer Method Biomed Eng 2013;29:1373–87. doi:10.1002/cnm.2588.

[16] LaDisa JF, Olson LE, Molthen RC, Hettrick DA, Pratt PF, Hardel MD, et al. Alterations in wall shear stress predict sites of neointimal hyperplasia after stent implantation in rabbit iliac arteries. Am J Physiol - Hear Circ Physiol 2005;288.

[17] De Nisco G, Kok AM, Chiastra C, Gallo D, Hoogendoorn A, Migliavacca F, et al. The Atheroprotective Nature of Helical Flow in Coronary Arteries. Ann Biomed Eng 2019. doi:10.1007/s10439-018-02169-x.

[18] Prati F, Gatto L, Romagnoli E, Limbruno U, Fineschi M, Marco V, et al. In vivo vulnerability grading system of plaques causing acute coronary syndromes: An intravascular imaging study. Int J Cardiol 2018;269:350–5. doi:10.1016/j.ijcard.2018.06.115.

[19] Steinman DA. Image-based computational fluid dynamics modeling in realistic arterial geometries. Ann Biomed Eng 2002;30:483–97. doi:10.1114/1.1467679.

[20] Chiastra C, Migliori S, Burzotta F, Dubini G, Migliavacca F. Patient-Specific Modeling of Stented Coronary Arteries Reconstructed from Optical Coherence Tomography: Towards a Widespread Clinical Use of Fluid Dynamics Analyses. J Cardiovasc Transl Res 2017. doi:10.1007/s12265-017-9777-6.

[21] Malvè M, García A, Ohayon J, Martínez MA. Unsteady blood flow and mass transfer of a human left coronary artery bifurcation: FSI vs. CFD. Int Commun Heat Mass Transf 2012. doi:10.1016/j.icheatmasstransfer.2012.04.009.

[22] Theodorakakos A, Gavaises M, Andriotis A, Zifan A, Liatsis P, Pantos I, et al. Simulation of cardiac motion on non-Newtonian, pulsating flow development in the human left anterior descending coronary artery. Phys Med Biol 2008. doi:10.1088/0031-9155/53/18/002.

[23] Zeng D, Ding Z, Friedman MH, Ross Ethier C. Effects of cardiac motion on right coronary artery hemodynamics. Ann Biomed Eng 2003. doi:10.1114/1.1560631.

[24] Torii R, Keegan J, Wood NB, Dowsey AW, Hughes AD, Yang GZ, et al. MR image-based

Post-print

geometric and hemodynamic investigation of the right coronary artery with dynamic vessel motion. Ann Biomed Eng 2010. doi:10.1007/s10439-010-0008-4.

[25] Chiastra C, Migliavacca F, Martínez MT, Malvè M. On the necessity of modelling fluid-structure interaction for stented coronary arteries. J Mech Behav Biomed Mater 2014;34. doi:10.1016/j.jmbbm.2014.02.009.

[26] Bukač M, Čanić S, Tambača J, Wang Y. Fluid–structure interaction between pulsatile blood flow and a curved stented coronary artery on a beating heart: A four stent computational study. Comput Methods Appl Mech Eng 2019. doi:10.1016/j.cma.2019.03.034.

Post-print

Figures

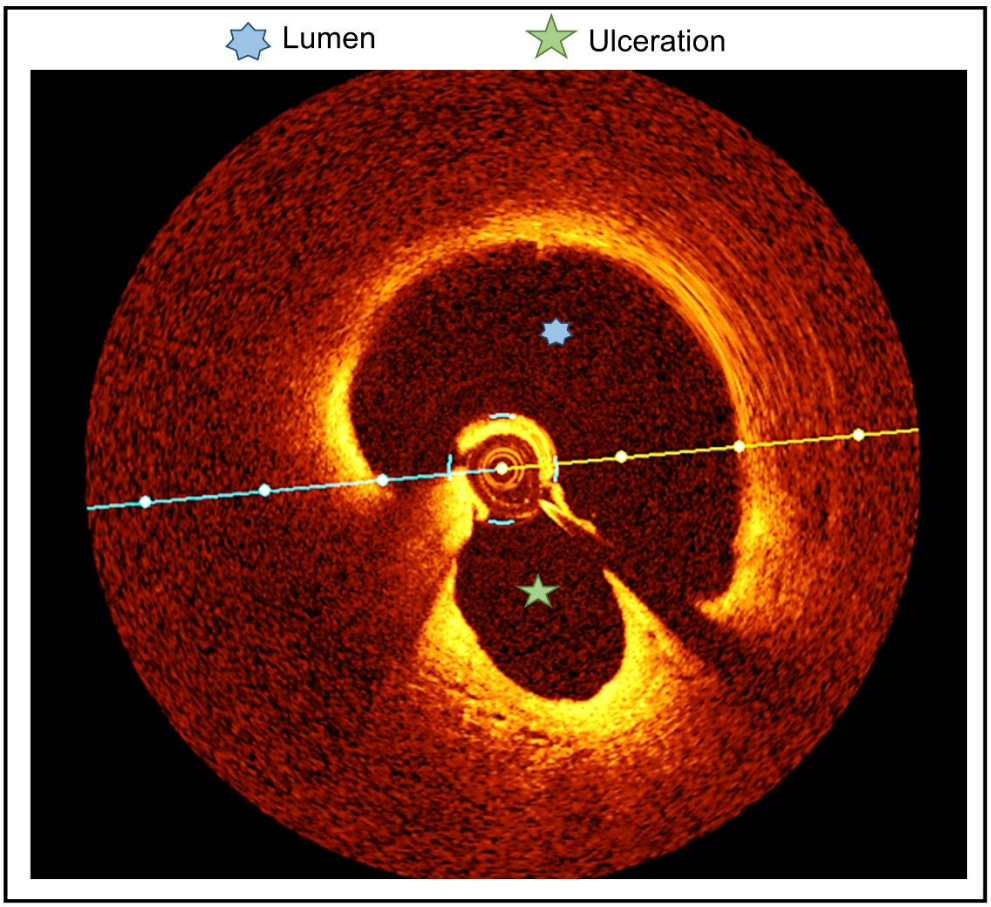

Figure 1.

Example of OCT frame at the ulcerated plaque in pre-operative diseased right coronary artery under investigation. The ulcerated plaque (five-pointed green star) besides the coronary artery lumen (seven-pointed blue star).

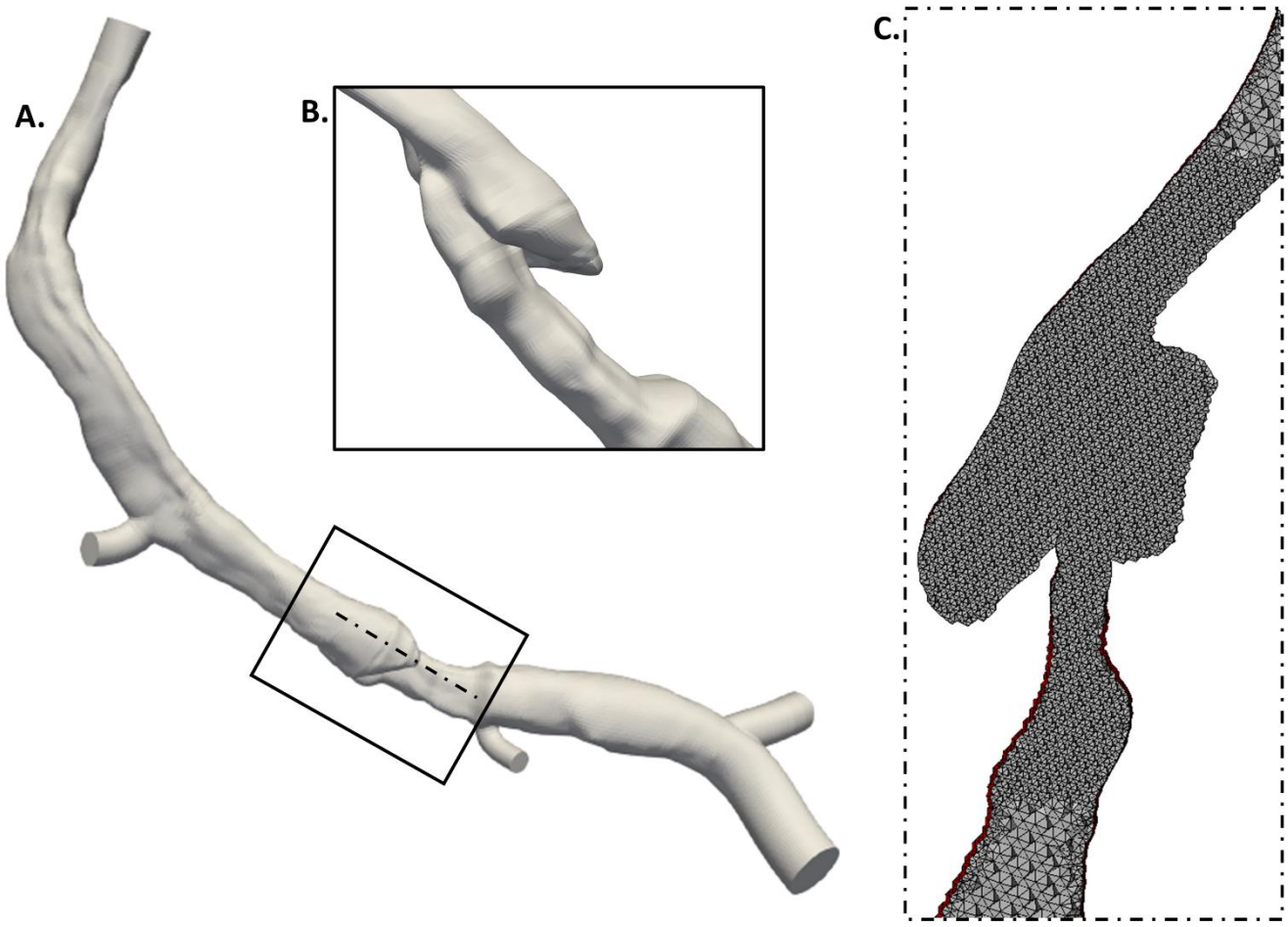

Figure 2.

3D reconstruction of a right coronary artery affected by plaque ulceration. A: 3D geometry. B: Detail of the ulcerated plaque. C: Longitudinal section of the volume fluid domain mesh, displaying higher element density at the plaque.

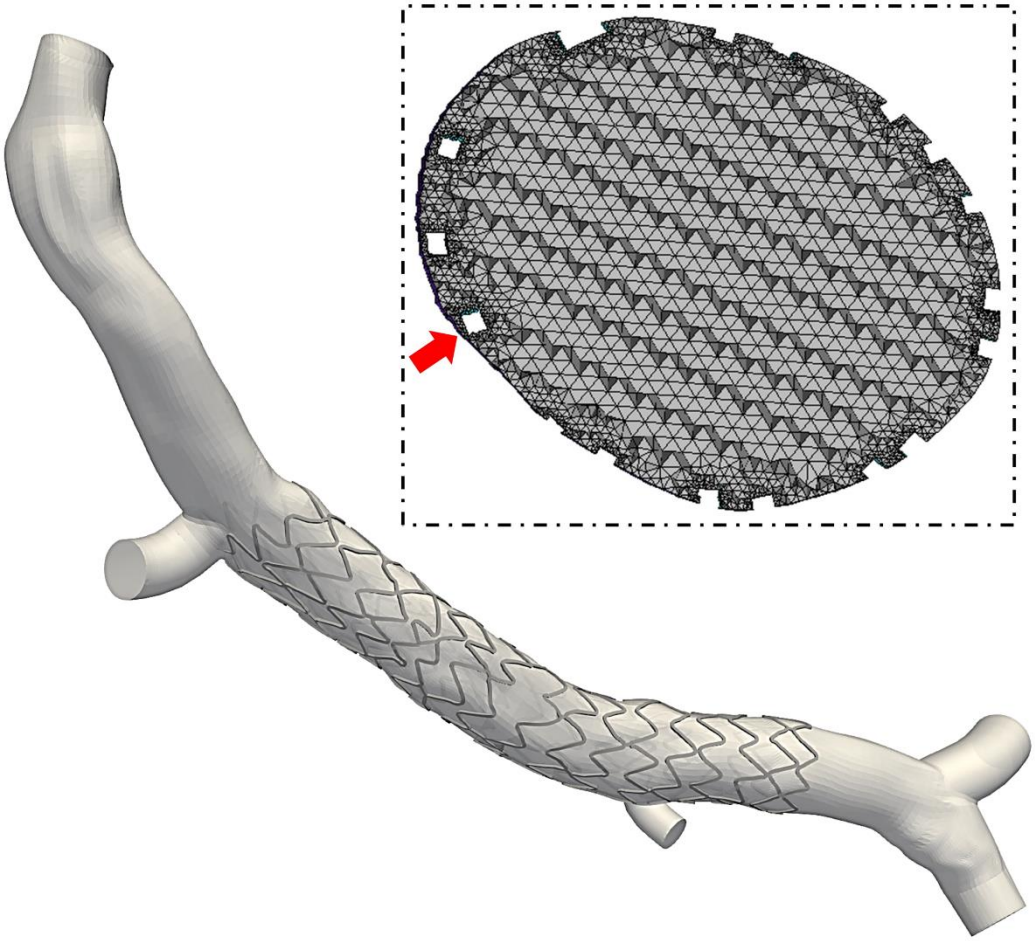

Figure 3.

3D reconstruction of the post-operative right coronary artery treated with the Nobori (Terumo) stent. A: 3D geometry. B: Cross-section of the volume fluid domain mesh. The malapposed stent struts, which are captured by the mesh, are indicated by a red arrow.

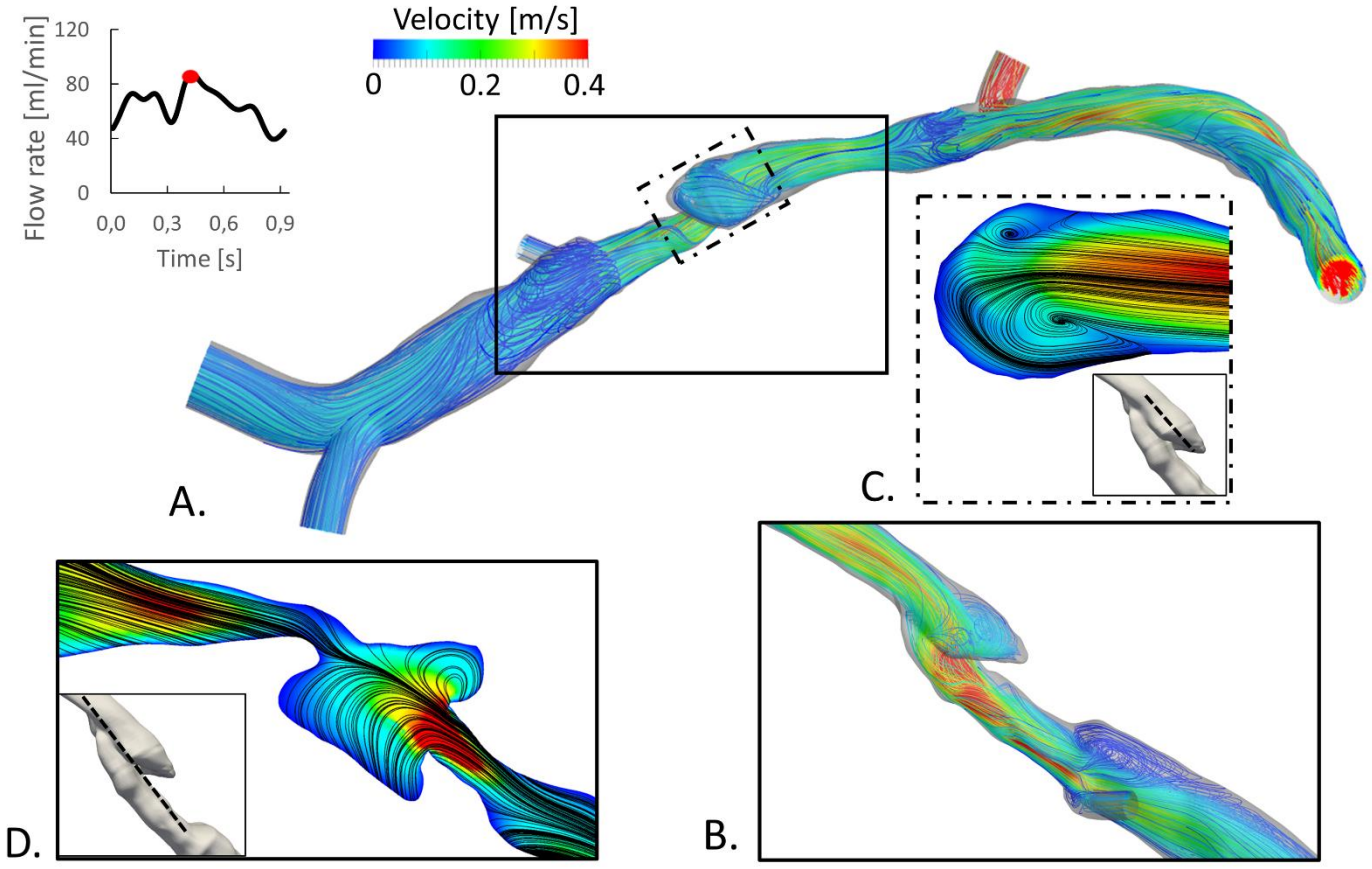

Figure 4.

Hemodynamic results of the pre-operative ulcerated case at peak for flow rate. A, B: Streamlines coloured by velocity magnitude. C, D: in-plane velocity contour maps with in-plane streamlines.

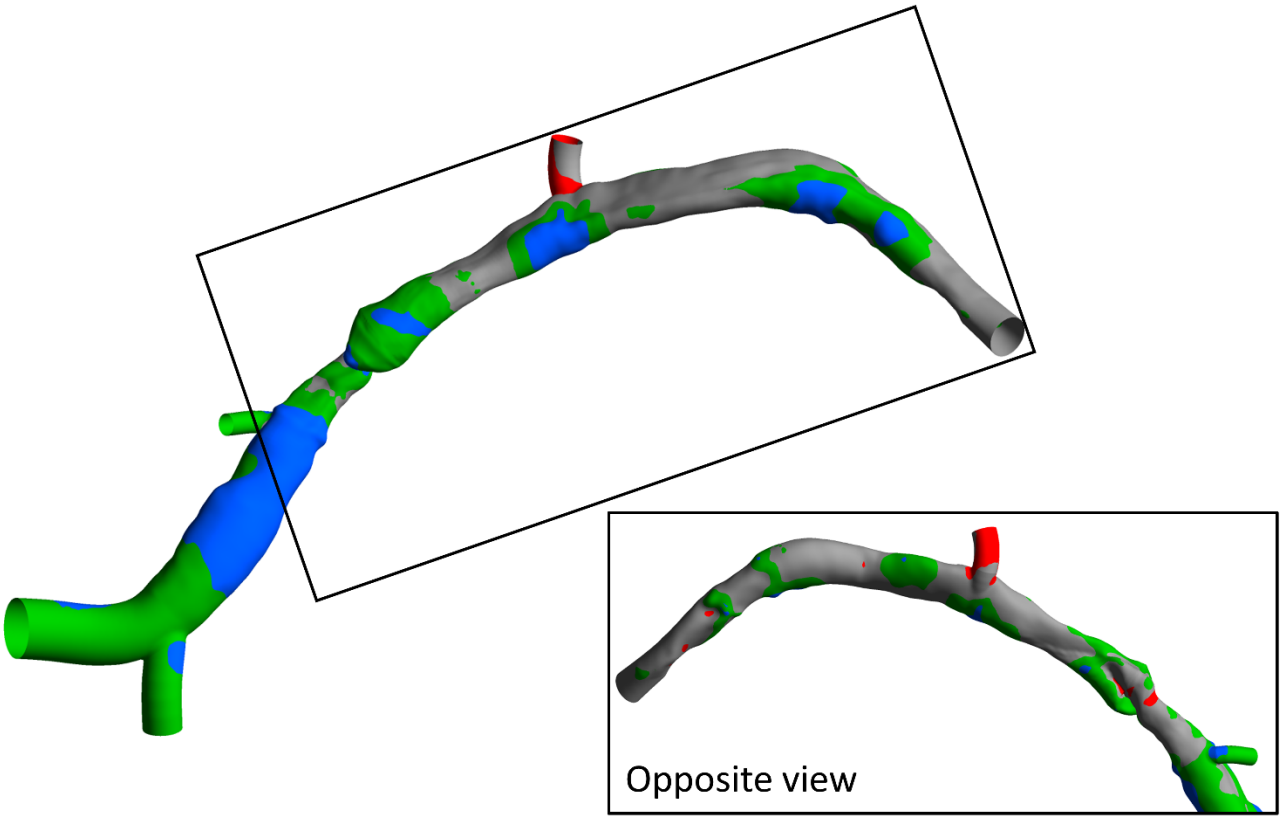

Lumen area [%]			
TAWSS < 0.4 Pa	0.4 Pa < TAWSS < 2 Pa	2 Pa < TAWSS < 10 Pa	TAWSS > 10 Pa
16.34	44.07	37.49	0.49

Figure 5.

Contour map showing intervals of the time-averaged wall shear stress (TAWSS) for the pre-operative ulcerated case.

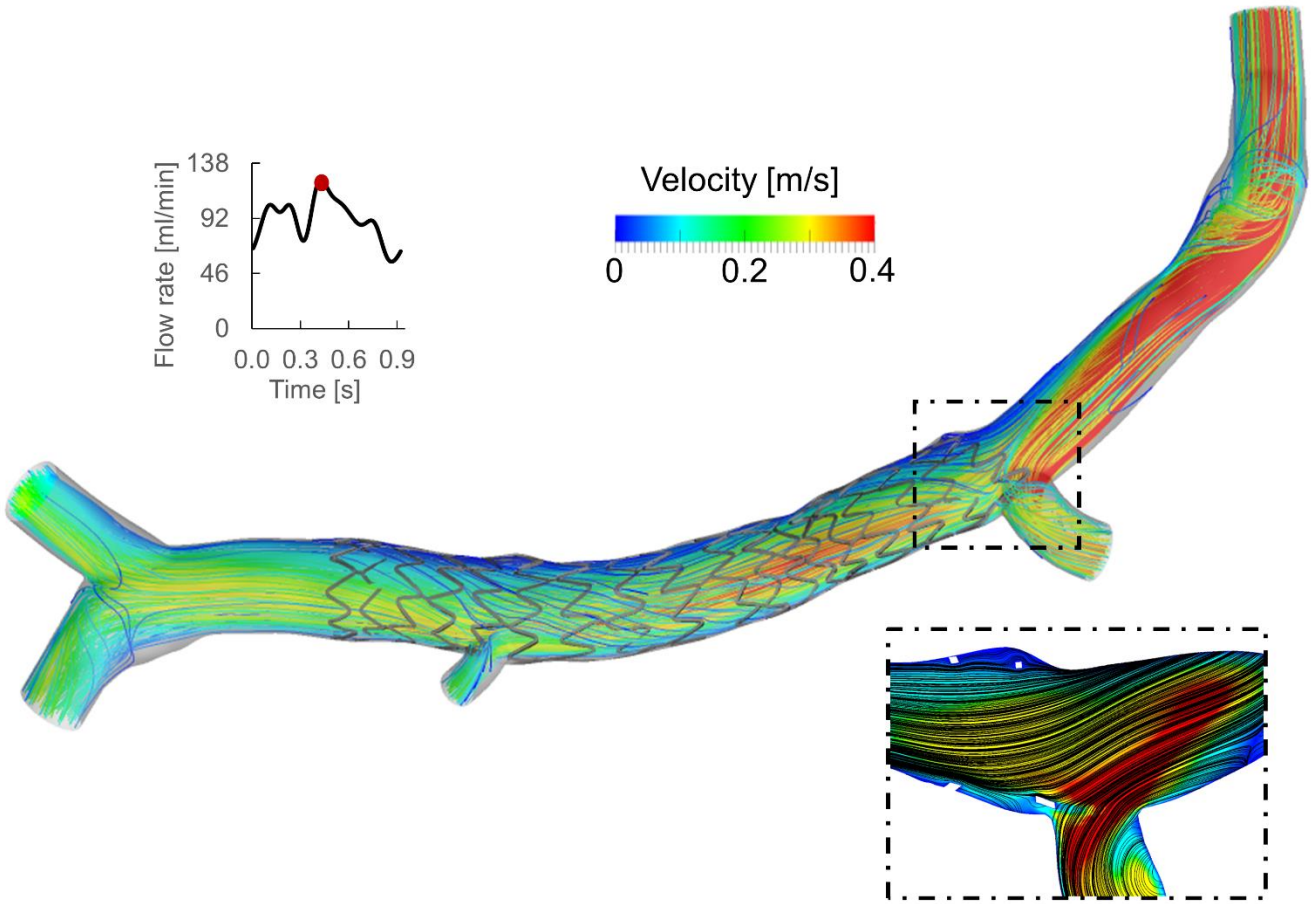

Figure 6.

Hemodynamic results of the ulcerated case after percutaneous coronary intervention at peak for flow rate. Streamlines of the velocity coloured by the velocity magnitude (top) and the in-plane velocity contour-map with in-plane streamlines (bottom).

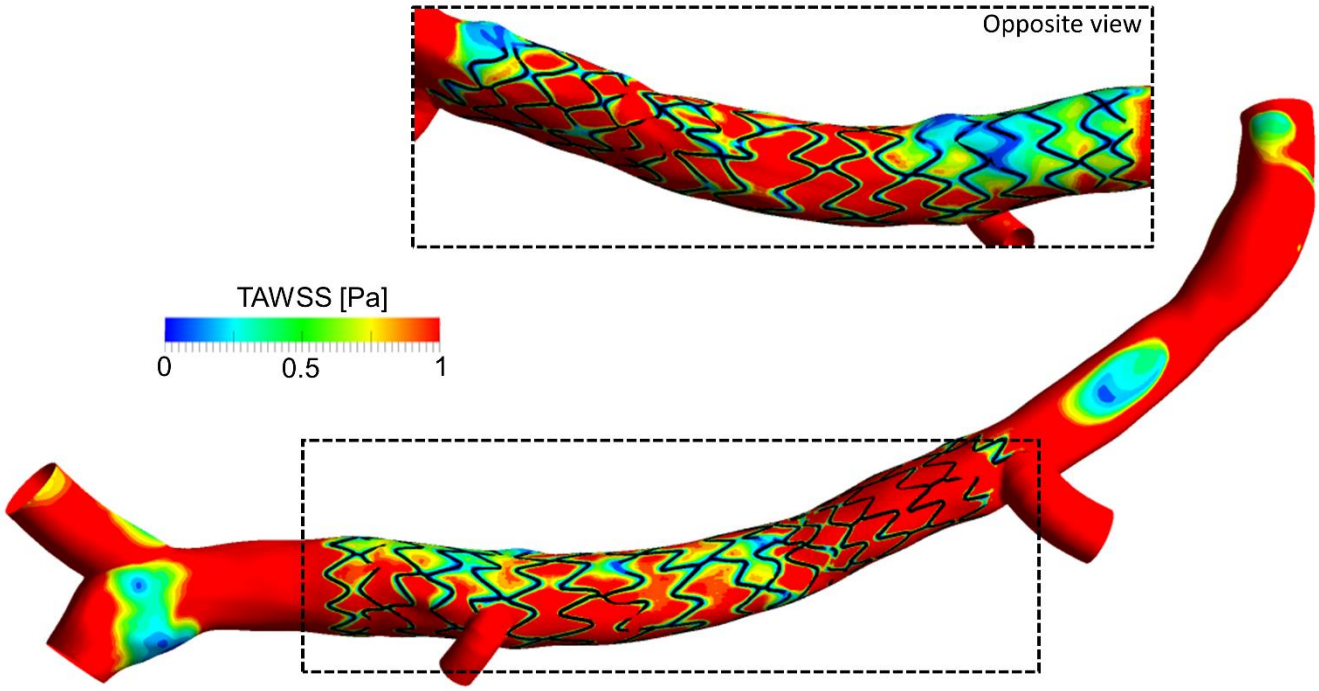

Figure 7.

Contour map of time-averaged wall shear stress (TAWSS) of the ulcerated case after percutaneous coronary intervention.